SAND98-1023J

Effects of spatially heterogeneous porosity on matrix-diffusion as investigated by X ray absorption imaging

Vincent C. Tidwell, Lucy C. Meigs, Tracy Christian-Frear, and Craig Boney

Sandia National Laboratories
Geohydrology Department
Albuquerque, New Mexico

Abstract: Laboratory experiments were performed to investigate the effects of spatial variation in porosity on matrix-diffusion processes. Four centimeter-scale slabs of Culebra dolomite taken from the Waste Isolation Pilot Plant site were used in the tests. Experiments involved the simple diffusion of iodine into a single edge of each rock slab while X ray absorption imaging was used to measure the resulting two-dimensional solute concentration field as a function of time. X ray imaging was also used to quantify the two-dimensional porosity field of each rock slab. Image analysis provided a unique opportunity to both visualize and quantify the effects of the spatially variable porosity on matrix-diffusion. Four key results were obtained. First, significant variation in rates of diffusion were realized over the relatively small length (centimeter) and time scales (months) investigated. Second, clear evidence of diffusion preferentially following zones of relatively higher porosity was noted. Third, rate of diffusion was found to vary as tracer diffused into the rock slabs encountering changing porosity conditions. Fourth, strong correlation between porosity and the calculated diffusion coefficients was found. In fact, the nature of the correlation can be related to the geometry, position, and orientation of the heterogeneous porosity features populating each rock slab.

1. Introduction

Predictive modeling of flow and transport in fractured rock requires careful consideration of matrix-diffusion processes (Neretnieks, 1980; Grisak and Pickens, 1980; Sudicky and Frind, 1982). This is because matrix-diffusion has the potential to both retard and disperse solutes traveling in the fracture network. Matrix-diffusion processes and their potential role in nuclear waste isolation has been extensively investigated at the Waste Isolation Pilot Plant (WIPP) site in southeastern New Mexico. Site-characterization studies have identified groundwater flow in the Culebra dolomite Member of the Rustler Formation as the most likely geologic pathway for radionuclide transport to the accessible environment in the event of a breach of the WIPP repository through inadvertent human intrusion. The Culebra is a 7-m-thick, variably fractured dolomite with massive and vuggy layers. Tracer tests performed in the Culebra (Meigs and Beauheim, 1998) have identified matrix-diffusion as an important transport process (Reeves et al., 1987; Jones et al., 1992; Altman et al., 1998). Numerical simulations of the tracer test data further indicate that some of the essential features of the data can be best explained by multiple rates of diffusion (Haggerty et al., 1998). The multiple rates occur as a result of variations in porosity type, in the tortuous nature of the pore structure, and in the size of matrix blocks (Haggerty et al., 1998).

Laboratory investigation of matrix-diffusion is being conducted on rock slabs collected from the Culebra dolomite. The purpose of these studies is to characterize the range and variability in diffusion coefficients associated with the Culebra dolomite and to gain a better understanding of the processes and media characteristics controlling diffusion. Here, we take a first step toward these goals by investigating the effects of spatial heterogeneity, as given by the two-dimensional porosity characteristics of the porous medium, on matrix-diffusion.

Many examples of laboratory studies have been reported in which diffusion coefficients were measured on crystalline rock (Garrels, et al., 1949; Bradbury et al., 1982; Wadden and Katsube,

DISCLAIMER

1982; Brady, 1983; Skagius and Neretnieks, 1986; Dykhuizen and Casey, 1989. Our work differs from these in that we employ X ray absorption imaging to both visualize and quantify the complex diffusion processes occurring in heterogeneous, two-dimensional rock slabs. With this technique both porosity and solute concentration, integrated over the medium's thickness, are measured at sub-millimeter spatial resolution. In this way, we are able to see how discrete features of the porosity field influence the spatial distribution of diffusion coefficients.

2. Methods and Materials

Simple forward diffusion (diffusion into the rock slabs) experiments were conducted on four centimeter-scale slabs of Culebra dolomite. Simple boundary conditions were employed to facilitate direct comparison of experimental results with that predicted by classical analytical models. Experiments progressed by subjecting a single edge of each rock slab to a source with constant tracer concentration. X ray images were then collected at selected time intervals throughout the test to visualize and quantify the diffusion process. Below, additional detail is given on the test cell design, X ray imaging procedure, data analysis, and the materials used in testing.

2.1 Test Cell Design

Each rock slab selected for testing was fitted with its own test cell (Figure 1). Bars of aluminum raw stock were cut to fit around the four edges of the rock slab and attached via machine screws. The aluminum frame was used to provide rigidity to the test cell and minimize X ray undercut around the edges of the sample. The aluminum frame and rock slab were then potted in epoxy. A high-viscosity epoxy was used to minimize imbibition into the rock. The epoxy was used to seal the faces of the rock slab along with two of the edges (edges were epoxied prior to assembly of the sample in the aluminum frame). Two opposing edges remained unepoxied to facilitate the saturating of the rock slab. During the diffusion experiments one of the unepoxied faces was sealed with a gasket while the other face served as the inlet for diffusion.

The finished test cells were mounted side by side on a steel bar to secure them in the same relative position from one image to another. A constant-density wedge (described below) was also mounted to the bar . To minimize density effects, the rock slabs were oriented horizontally throughout the diffusion experiments.

For each test cell, a fluid reservoir was milled into one of the aluminum end pieces coincident with an unepoxied face. A constant tracer concentration boundary condition was achieved by circulating fluid through the reservoir. Flow rates were maintained low so as to avoid positive fluid pressures in the reservoir while still sufficient to maintain a tracer concentration in the reservoir to within 1% of the desired level. For the first three days of the experiment fluid, was supplied to each sample at an approximate rate of 0.80 mL/min., which was incrementally reduced to 0.16 mL/min. by the fifth day. Fluid was circulated using a peristaltic pump that pumped fluid from an upstream reservoir to each individual test cell reservoir and out to individual downstream reservoirs. Tracer concentrations in the upstream and downstream reservoirs were continuously monitored as was the mass of fluid pumped through each test cell. The average concentration in both the upstream and downstream reservoirs, as measured with an ion-specific probe, was 1.0×10^5 mg/L KI with a standard deviation of 1.5×10^3 mg/L.

Temperatures within the laboratory averaged 21°C with a standard deviation of 0.6°C throughout the duration of the diffusion experiments.

2.2 X ray Imaging

High-resolution tracer-concentration images were acquired by directing a beam of X rays at the face of the rock slabs while recording the transmitted intensity field on film secured in a cassette behind the test system. The transmitted X ray intensity recorded at each point is a function of the

density of the rock, integrated over the full thickness of the slab. Thus, variations in the transmitted X ray intensity field arise from the spatially varying porosity characteristics of the rock slab as well as differences in tracer concentration.

The X ray source, rock slabs, and film cassette were mounted in a rigid frame for imaging. A source-to-target distance of 2.5 m and a target-to-film distance of 1.25 cm were used so as to minimize distortion of the image. The X ray source intensity used in imaging was tuned to the absorption characteristics of the tracer. The iodide ion in the form of potassium iodide (KI) was used as the solute tracer. KI was selected because it is geochemically conservative and has favorable X ray absorption characteristics. For KI a source potential of 60 kV and tube current of 27 mA were used. The accompanying exposure time, as determined by trial and error, was set so as to maximize image contrast which is a function of sample thickness, sample porosity, and tracer concentration. For this experiment an exposure time of 7.5 minutes was used.

The exposed X ray film was developed after each shot. The bulk X ray film density changes from film to film because of variations in the source intensity, film quality, and the film developing process. To account for this variation, a constant-density wedge was included in every image. The wedge, which varies linearly in thickness from 0 to 0.63 cm, was made of a hardened epoxy/tracer mixture. The tracer concentration suspended in the wedge was the same as used in the diffusion experiment.

2.3 Digitizing the X ray Images

Spatial variation in solute concentration within each rock slab is recorded as differences in film density. To quantify these differences digital imaging is employed. This is accomplished by placing the developed X ray film in front of a computer-controlled, diffused bank of high-frequency (60 MHz), high-output fluorescent lights. Variation in the transmitted light intensity field, corresponding to differences in film density and, hence, the solute concentration, is recorded by means of a CCD (charge-coupled device) camera focused on the front of the X ray film. The CCD camera output is digitized into an array of 1024 by 1024 points, with each point assigned a gray-level value between zero and 4095 according to the transmitted light intensity. The array size of the camera and the size of the test system determine the spatial resolution of the acquired image. For these tests the spatial resolution is 0.25 by 0.25 mm per pixel.

As part of the imaging process, each film must be aligned with respect to all other imaged films. To aid in this process, two lead reference marks are affixed in opposite corners of each rock slab. Coarse alignment is achieved by hand while fine tuning is accomplished through image processing.

2.4 Data Reduction and Analysis

To determine relative tracer concentration from the digitized images, gray-level values are converted through a two-step process. The first step adjusts the image according to the constant density wedge included in each image to correct for variations in the source (X ray and light) intensity, film quality, and the film developing process. The second step takes the adjusted gray-level values and converts them to values of relative concentration. Here we assume linear absorption governs the transmission of X rays through the rock slabs and, likewise, linear absorption governs the transmission of light through the developed X ray film. The resulting model for calculating the relative concentration, C/C_o, from the gray-level data is (Tidwell and Glass, 1994)

$$\left(\frac{C}{C_o}\right)_{i,j} = \frac{\ln(I)_{i,j} - \ln(I_d)_{i,j}}{\ln(I_s)_{i,j} - \ln(I_d)_{i,j}} \qquad (1)$$

where C_o is the inlet tracer concentration, I is the transmitted light intensity at a given point (located at coordinates i, j), I_s is the transmitted light intensity at the same point in the image for the fully saturated tracer condition (image $C/C_o = 1$), and I_d is the transmitted light intensity at the same point in the image at the start of the test before tracer has diffused into the rock slab (image $C/C_o = 0$). By applying Equation 1 at each point or pixel in the image domain the two-dimensional relative-concentration field is calculated. Visualization and quantification of matrix-diffusion processes is achieved by simply repeating this procedure for the time-sequenced series of images acquired over the duration of the test.

Two-dimensional porosity fields at the same spatial resolution as the relative-concentration fields are also calculated for each rock slab. The porosity at each pixel, $\phi_{i,j}$, is determined from the X ray images taken of the tracerless and tracer saturated samples according to the relation

$$\phi_{i,j} = \frac{\ln(I_s)_{i,j} - \ln(I_d)_{i,j}}{E\left[\ln(I_s)_{i,j} - \ln(I_d)_{i,j}\right]} \bar{\phi} \frac{z_{i,j}}{Z_{avg}} \tag{2}$$

were $E\left[\ln(I_s)_{i,j} - \ln(I_d)_{i,j}\right]$ is the average difference between the tracer saturated and tracerless images, $\bar{\phi}$ is the bulk porosity of the rock slab measured by gravimetric means, z_{avg} is the average thickness of the rock slab, and $z_{i,j}$ is the rock slab thickness at each pixel estimated from measurements made with calipers on the corners of the rock slab to which a simple trend surface is fit.

To investigate matrix-diffusion processes the normalized cumulative mass, M_t/M_∞, is calculated. We define M_t as the cumulative mass of tracer diffused into the porous medium at time t and M_∞ as the corresponding quantity at $t = \infty$ (i.e., when each pixel reaches a concentration equal to C_o). These calculations are performed along transects oriented normal to the input face. M_t/M_∞ is calculated or each relative-concentration image according to the relation

$$\left(\frac{M_t}{M_\infty}\right)_j = \frac{\sum_{i=1}^{N}\left(\frac{C}{C_o}\right)_{i,j} z_{i,j}\phi_{i,j}}{\sum_{i=1}^{N} z_{i,j}\phi_{i,j}} \tag{3}$$

where N is the number of pixels in a transect spanning the full length l of the rock slab. Calculations are performed over transects one pixel wide (as given in Equation 3), the width of the sample, and other intermediate widths.

Diffusion experiments were conducted by prescribing a constant tracer concentration boundary condition along one edge of the rock slab while diffusion was prevented across all other boundaries. This configuration allows direct comparison with analytical solutions for one-dimensional diffusion in a finite slab. According to Crank (1975) the normalized cumulative mass is given by

$$\frac{M_t}{M_\infty} = 1 - \sum_{n=0}^{\infty} \frac{8}{(2n+1)^2\pi^2} \exp\left[\frac{-D(2n+1)^2\pi^2 t}{4l^2}\right] \tag{4}$$

where D is the diffusion coefficient, l is the slab length, and n the iteration step. Important assumptions made in this solution are that the diffusion coefficient is constant, the porous medium is homogeneous and isotropic, the tracer is conservative, and the boundary conditions are constant throughout the test.

Inversion and truncation of Equation 3 provides a direct means of calculating D from the M_t/M_∞ profile. Crank (1975) gives the relation

$$D = \frac{0.196l^2}{t_{0.5}} \tag{5}$$

where $t_{0.5}$ is the time at which $M_t/M_\infty = 0.5$. The error caused by the truncation is reported to be approximately 0.001%.

2.5 Sample Selection and Preparation

Four Culebra dolomite samples with differing physical attributes were chosen for use in the diffusion experiments. These samples were selected according to their representativeness of the porosity forming features found within the Culebra dolomite. Here we focus on the porosity occurring within the crystalline dolomite, the porosity formed by fractures and vugs, and the porosity reducing gypsum-fillings that occur in many of the fractures and vugs. A brief description of the rock slabs is given in Table 1. A more detailed geologic description of the Culebra dolomite can be found in Holt (1997).

Prior to testing, the samples were cut into thin rock slabs. Efforts were made to cut the samples such that the primary physical attributes of the sample were oriented normal to the slab faces and were continuous throughout the thickness of the sample. The length and width of the slabs were selected so as to encompass a sufficient degree of "heterogeneity" in each sample while keeping the samples small with respect to the time and spatial scales of the diffusion process. Thickness of the slabs was selected to optimize X ray image contrast. Pre-test evaluation (imaging of slabs of different thicknesses saturated with different tracer concentrations) indicated an optimal thickness of 2.5 cm.

2.6 Aqueous Phase

Groundwater from the Culebra dolomite is characterized as a brine. Although predominately sodium chloride (NaCl), the detailed composition and concentration varies significantly across the WIPP site. To maintain some consistency a brine was used for the background aqueous phase in the diffusion studies; however, given its inherent variability at the WIPP site we did not attempt to make a rigorous match. Rather, a simple sodium chloride (NaCl) solution was selected with a concentration set so as to maintain molar strength equilibrium with the KI tracer. Pre-test experiments showed that good X ray image contrast was achieved with an iodide concentration of 1.0×10^5 mg/L or a molar concentration of 0.79 molar. Thus, the rock slabs were initially saturated with the 0.8 molar NaCl brine while the tracer fluid consisted of both the 0.8 molar NaCl brine and the 0.79 molar KI.

3. Results

3.1 Diffusion Images

Diffusion experiments were allowed to proceed for almost 45 days. During this period of time 15 images were acquired. Image times were distributed according to a linear function of the square root of time. Figures 2-5 present visual and quantitative data for the transient diffusion of KI into the Culebra samples at selected times. For each sample the two-dimensional relative KI

concentration field is given at a spatial resolution of approximately 0.0625 mm^2 (from 15,000-30,000 points per sample). In addition, the porosity image is given at the same spatial resolution.

Inspection of the time-sequenced series of images clearly reveals smooth (in time) and consistent diffusion of KI into each of the rock slabs. More importantly, a distinct relationship between the spatial characteristics of the porosity field and the diffusion of KI is evident. For sample RC1-A (Figure 2), the concentration front remains relatively uniform throughout the diffusion process reflecting its almost featureless porosity field. However, slight asymmetry is present in the concentration front centered on the laminae faintly visible in the porosity field. Similarly, the fracture in sample RC2-B (Figure 3) is seen to be the point of focused solute diffusion until later times when the concentration front reaches the end of the fracture. The increased porosity in the right-hand side of sample B33-H (Figure 4) is likewise seen to skew the tracer distribution. In sample RC6-G (Figure 5), only local variation in the concentration front is evident. The lack of broad trends results from the primary porosity features being oriented normal to the direction of diffusion. Specifically, the gypsum-filled vug (near the center of the rock slab) and the open, high-porosity vug (opposite the inlet boundary) are oriented parallel to the inlet and nearly span the full width of the rock slab.

Comparisons have also been drawn between the X ray porosity images and the physical attributes of the Culebra rock slabs. Visual aspects of each sample (i.e., vugs, lamination) are easily correlated with features in the measured porosity field. The one exception is the fracture in sample RC2-B (Figure 3), which is only faintly visible in the porosity image because of its oblique orientation to the imaging plane.

Along with the visual aspects of the X ray images, quantification of the porosity, solute concentration, and rate of diffusion (discussed later) has been accomplished. An error analysis has not been performed on the acquired data set because the nature of the experiment did not allow for a direct and independent means of measuring the solute mass in the samples as a function of time. However, previous studies have found the method to be accurate to ±5% in the measured state variable (Tidwell and Glass, 1994).

3.2 Rate of Diffusion Versus Time

The two-dimensional relative-concentration fields (Figures 2-5) show a distinct relationship between the spatially heterogeneous porosity characteristics of each rock slab and the diffusional process. Here, we explore the effect of heterogeneity on the rate of diffusion. To aid in this we investigate the behavior of the normalized cumulative mass, M_t/M_∞, (Equation 3) as a function of time. For each rock sample, M_t/M_∞ vs. $t^{1/2}$ profiles are presented for selected intervals five pixels wide and integrated over the full width of the rock slab (Figure 6). The measured M_t/M_∞ vs. $t^{1/2}$ profiles are then compared to that predicted assuming a constant diffusion coefficient (Equation 4). Differences in the measured and predicted profiles are interpreted in terms of the effects of heterogeneity encountered by the tracer as it diffuses into the rock slab.

A discontinuity in the M_t/M_∞ vs. $t^{1/2}$ profiles at early times is evident in each data set. The discontinuity was caused by difficulties in fully purging the fluid delivery system of tracerless brine solution prior to testing (the system was initially operated with tracerless brine solution to test for leaks) and the inadvertent entry of air bubbles into the sample reservoirs at the beginning of the experiment. Once recognized, steps were taken to rectify the problem. To account for this problem, the modeled M_t/M_∞ vs. $t^{1/2}$ profiles were generated using a time-dependent boundary condition (Crank, 1975).

Each of the four rock slabs exhibit somewhat different behavior. For sample B33-H the modeled and measured normalized cumulative mass profiles (Figure 6c) agree quite closely, reflecting the relatively uniform porosity distribution characterizing the rock slab. Although sample RC1-A also

exhibits a relatively uniform porosity distribution, a distinct discontinuity (t=1.6 to 2.5×10^5 sec) in the normalized cumulative mass profiles is noted for all three curves (Figure 6a). Specifically, an initially high rate of diffusion is followed by an abrupt change to a rate that is only half the previous rate. In part, this discontinuity may be the result of instability in the boundary conditions. However, an important contributor to this discontinuity is believed to be the relatively high porosity focused near the inlet to the rock slab (Figure 2).

The normalized cumulative mass profiles for sample RC2-B (Figure 6b) clearly reflect the effect of the fracture on the rate of diffusion (Figure 3). One profile was taken near the fracture while a second was taken near the far right-hand side of the slab. Near the fracture the rate of diffusion starts high but then drops (after $t=2.5 \times 10^5$ sec) by over an order of magnitude once the tracer reaches the end of the fracture. In contrast, neither the profile near the right-hand side of the slab nor the integrated profile show much effect of the fracture. In fact, both are fit quite well by a single rate of diffusion, owing to the relatively uniform porosity of the rock slab away from the fracture.

Diffusion into sample RC6-G (Figure 6d) is seen to follow a relatively uniform rate except during intermediate times ($t=8.1\text{-}12.1 \times 10^5$ sec). Similar behavior is seen for both selected transects and the profile for the integrated sample. This behavior results from diffusion at intermediate times being impeded by the gypsum-filled vug (the gypsum is characterized by low porosity [Figure 5], and thus a relatively low diffusion coefficient). At early times the rate of diffusion decreases as the front approaches the gypsum-filled vug; however, the tracer concentration upstream of the vug grows. As the concentration grows the gradient across the vug becomes very steep which leads to an effective increase in the rate of diffusion. The relatively high porosity of the rock slab beyond the gypsum-filled vug further facilitates the diffusion process in this part of the sample.

In summary, Figure 6 shows that the rate of diffusion is sensitive to the heterogeneities encountered along the path of tracer transport. Where the media is relatively homogeneous, a single-rate of diffusion governs the migration of the solute tracer. Alternatively, where significant changes in porosity are encountered (e.g., fracture, gypsum-filled vug), corresponding changes in the rate of diffusion occur.

3.3 Comparison of Diffusion Coefficients

To compare diffusional behavior for different rock samples and, thus different heterogeneous features, diffusion coefficients were calculated from the measured relative mass data (Equation 3) using Equation 5. We recognize that this simple model fails to account for many important processes that we have already shown to influence diffusion (i.e., heterogeneity in the porosity, two-dimensional diffusion, time-varying boundary conditions as encountered early in the experiment). Nevertheless, by employing the same measure (i.e., Equation 5) for all samples a consistent basis by which to compare the diffusional characteristics is obtained. As such, emphasis is placed not on the individual values but rather on the relative differences in the calculated diffusion coefficients.

Diffusion coefficients calculated from the X ray image data are plotted as a function of position (parallel to the inlet boundary of the rock slab) for all four rock slabs (Figure 7). The diffusion coefficients vary by almost a order of magnitude among the four samples and by a factor of 2-3 within samples. Much of the variability in the diffusion coefficients can be related to physical features of the rock slabs. For example, RC1-A exhibits a relatively uniform porosity field (Figure 2) and hence a near uniform distribution of diffusion coefficients. Diffusion coefficients for RC2-B exhibit a steady increase in magnitude as the distance from the fracture decreases. Similarly, the diffusion coefficients for B33-H steadily increase from left to right across the rock slab consistent with the increasing vug concentration (Figure 4). Finally, the diffusion coefficients are noted to increase from right to left across sample RC6-G reflecting the thinning of the cross-cutting gypsum-filled vug (Figure 5).

To further explore the relationship between diffusion and the heterogeneous features of the rock slabs, scatter plots of the porosity versus the calculated diffusion coefficients were plotted (Figure 8). These plots compare the diffusion coefficients calculated along transects one pixel wide and the full width of the sample (average bulk parameters) with the corresponding arithmetically averaged porosity. Three of the four scatter plots are seen to yield a strong correlation between porosity and the diffusion coefficient. More importantly, the nature of the correlation between the four samples differs significantly. In fact, these differences may well be indicative of the influence of media heterogeneity on matrix-diffusion. RC1-A reveals a relatively uniform distribution of diffusion coefficients even though the porosity varies from approximately 0.11 to 0.15. These variations in porosity have little effect on diffusion because the higher porosities are concentrated near the inlet boundary and thus their effect is quickly stabilized by the relatively uniform porosity encountered deeper into the rock slab. The correlation shown by RC2-B can be related to the fracture. Although the fracture has little influence on the porosity it has significant effect on diffusion as it is well connected to the inlet boundary. This is reflected by the near parabolic shape of the scatter plot. For B33-H, the magnitude of the diffusion coefficient is closely correlated with the vug concentration, which gives rise to a nearly linear correlation between porosity and the diffusion coefficient. RC6-G, on the other hand, lacks strong correlation between porosity and the diffusion coefficient. This lack of correlation is interpreted as the result of the primary structural features (gypsum-filled vug and high-porosity vug near the outlet) being disconnected from the inlet boundary and oriented normal to the direction of diffusion.

In contrast, poor correlation between the porosity and diffusion coefficient was found for the bulk sample values (Figure 8). This result, in conjunction with the correlations drawn above, suggest that diffusion does not simply depend on the magnitude of the porosity but also depends on how it is spatially distributed. In these tests the spatial pattern, size, connectedness, and orientation (with respect to direction of diffusion) of the heterogeneous porosity features have been seen to influence diffusion.

4. Conclusions

Simple forward diffusion studies were conducted on four centimeter-scale slabs of Culebra dolomite. X ray absorption imaging was used to visually and quantitatively investigate the effect of matrix heterogeneity, as exhibited by the spatially varying properties of the porosity field, on the diffusion characteristics of a conservative tracer. Clear and unique relationships between the porosity and diffusion characteristics were demonstrated for each rock sample. These trends were manifest in three different ways. First, the two-dimensional tracer-concentration fields acquired by X ray imaging showed preferential diffusion in zones of high relative porosity. Second, the normalized cumulative-mass profiles exhibited non-uniform diffusion characteristics that correspond to heterogeneities encountered by the tracer as it diffused into the rock slabs. Third, scatter-plots between the calculated diffusion coefficients and arithmetically averaged porosity show surprisingly strong correlation. In fact, the nature of the correlation can be attributed to the geometry, position, and orientation of the heterogeneous porosity features populating each rock slab. These results are significant as they provide strong physical evidence that the spatial characteristics of the porosity field influence diffusional processes. Furthermore, these results demonstrate that considerable variation in diffusion processes occurs over spatial scales of centimeters and temporal scales of months.

Acknowledgments: The authors would like to recognize a number of individuals who contributed to this work. We thank Robert Glass for valuable guidance provided early in the development of this project, Robert Holt for insight on Culebra geology, Santiago Pons for constructing the flow cells, Jack Istok (Oregon State University) for help with preparing the test system, fluid chemistry measurements and performing preliminary imaging, and Roy Haggerty

(Oregon State University) for assistance with the data analysis. This work was funded by the Waste Isolation Pilot Plant program, U.S. Department of Energy. Sandia is a multiprogram laboratory operated by Sandia Corporation, a Lockheed Martin Company, for the United States Department of Energy under Contract DE-AC04-94AL85000.

References

Altman, S.J., L.C. Meigs, T.L. Jones, Y Tsang, Tracer tests in a fractured dolomite: 2. Evaluation of he importance of matrix diffusion, submitted to *Water Resour. Res.*, 1998.

Bradbury, M.H., D. Lever, and D. Kinsey, Aqueous phase diffusion in crystalline rock, *in Scientific Basis for Nuclear Waste Management V,* 11, 569-578, Elsevier, New York, 1982.

Brady, J.B., Intergranular diffusion in metamorphic rocks, *Amer. Jour. Sci.,* 283, 181-200, 1983.

Crank, J., *The Mathematics of Diffusion*, Clarendon Press, Oxford, 1975.

Dykhuizen, R.C. and W.H. Casey, An analysis of solute diffusion in the Culebra dolomite, *SAND89-0750*, Sandia National Laboratories, Albuquerque, New Mexico, 1989.

Garrels, R.M., R.M. Dreyer, and A.L. Howland, Diffusion of ions through intergranular space in water-saturated rocks, *Bull. Geol. Soc. Am.,* 60, 1809-1828, 1949.

Grisak, G.E., and J.F. Pickens, Solute transport through fractured media: 1, The effect of matrix diffusion, *Water Resour. Res.,* 16(4), 719-730, 1980.

Meigs, L.C. and R.L. Beauheim, Tracer tests in a fractured dolomite: 1. Experimental design and observed tracer recoveries, *Water Resour. Res.,* 1998.

Neretnieks, I., Diffusion in the rock matrix: An important factor in radionuclide retardation, *J. Geophys. Res.,* 85(B8), 4379-4397, 1980.

Haggerty, R., S.W. Fleming, L.C. Meigs, and S.A. McKenna, Convergent-flow tracer tests in a fractured dolomite: 3. Analysis of mass transfer in single-well injection-withdrawal tests, submitted to *Water Resour. Res.*, 1998.

Holt, R.M., Conceptual model for transport processes in the Culebra Dolomite Member, Rustler Formation, *SAND97-0194*, Sandia National Laboratories, Albuquerque, NM, 1997.

Jones, T.L., V.A. Kelley, F.F. Pickens, D.T. Upton, R.L. Beauheim, and P.B. Davies, Integration of Interpretation Results of Tracer Tests Performed at the Waste Isolation Pilot Plant Site, SAND92-1579, Sandia National Laboratories, Albuquerque, NM, 1992.

Reeves, M., V.A. Kelley, and J.F. Pickens, *Regional Double-Porosity Solute Transport in the Culebra Dolomite: An Analysis of Parameter Sensitivity and Importance at the Waste Isolation Pilot Plant (WIPP) Site*, SAND87-7105, Sandia National Laboratories, Albuquerque, NM, 1987.

Skagius, K. and I. Neretnieks, Porosities and diffusivities of some nonsorbing species in crystalline rocks, *Water Resour. Res.*, 22(3), 389-398, 1986.

Sudicky, E.A. and E.O. Frind, Contaminant transport in fractured porous media: Analytical solutions of a system of parallel fractures, *Water Resour. Res.,* 18(6), 1634-1642, 1982.

Tidwell, V. C. and R. J. Glass Jr., X ray and visible light transmission for laboratory measurement of two-dimensional saturation fields in thin-slab systems, *Water Resour. Res.*, 30(11), 2873-2882, 1994.

Wadden, M.M. and T.J. Katsube, Radionuclide diffusion rates in igneous crystalline rocks, *Chem. Geol.*, 36, 191-214, 1982.

Table 1. Rock slab descriptions.

Sample	Length (cm)	Width (cm)	Thickness (cm)	Porosity	Description
RC1-A	4.9	4.9	2.5	0.13	Featureless gray dolomite with single faint laminae oriented parallel to direction of diffusion.
RC2-B	6.6	4.2	2.5	0.09	Featureless gray dolomite with a distinct fracture. Fracture extends from inlet boundary to near the center of the rock slab (~3.8 cm long). Fracture traverses full thickness of the rock slab at oblique angle to slab face.
B33-H	5.5	4.8	2.6	0.15	Vuggy gray dolomite. Vugs range in size from 0.025 to 0.25 cm and are locally interconnected and/or interconnected through fractures. Some vugs are filled with gypsum.
RC6-G	6.2	4.2	2.5	0.12	Vuggy and fractured gray dolomite with partial gypsum filling. Vugs range in size from 0.025 to 2.0 cm. A single large vug filled with gypsum crosscuts the sample approximately 1.2 cm from the inlet surface. The gypsum-filled vug is 1.2 cm wide and spans much of the width and thickness of the rock slab. Numerous fractures filled with gypsum emanate from the large gypsum vug.

Figure Captions

Figure 1. Test cell schematic.

Figure 2. Relative concentration fields measured by X ray absorption imaging showing the diffusion of a KI tracer into a brine-saturated slab of Culebra Dolomite. Also shown is the two-dimensional porosity field. Pictured is sample RC1-A characterized by relatively uniform intercrystalline porosity.

Figure 3. Relative concentration fields measured by X ray absorption imaging showing the diffusion of a KI tracer into a brine-saturated slab of Culebra Dolomite. Also shown is the two-dimensional porosity field. Pictured is sample RC2-B characterized by relatively uniform intercrystalline porosity cut by a single fracture running from the inlet to approximately half the length of the sample.

Figure 4. Relative concentration fields measured by X ray absorption imaging showing the diffusion of a KI tracer into a brine-saturated slab of Culebra Dolomite. Also shown is the two-dimensional porosity field. Pictured is sample B33-H characterized by an intercrystalline matrix containing numerous open vugs.

Figure 5. Relative concentration fields measured by X ray absorption imaging showing the diffusion of a KI tracer into a brine-saturated slab of Culebra Dolomite. Also shown is the two-dimensional porosity field. Pictured is sample RC6-G characterized by an intercrystalline matrix containing numerous open and gypsum-filled fractures and vugs.

Figure 6. Normalized cumulative mass (symbols), M_t/M_∞, plotted as a function of $t^{1/2}$ for sample a) RC1-A, b) RC2-B, c) B33-H, and d) RC6-G. Shown are profiles for two selected intervals five pixels wide (see corresponding porosity image for location [Figures 2-5]) and the M_t/M_∞ profile averaged over the entire width of the rock slab. Also shown are M_t/M_∞ vs. $t^{1/2}$ (solid and dashed curves) profiles assuming a constant diffusion coefficient (Equation 4) and time-varying input boundary conditions (at early times only).

Figure 7. Diffusion coefficient (Equation 5) versus position along the inlet boundary for samples RC1-A, RC2-B, B33-H, and RC6-G. The reported diffusion coefficients were calculated for transects measuring one pixel in width.

Figure 8. Scatter-plots of porosity verses diffusion coefficient for samples RC1-A, RC2-B, B33-H, and RC6-G (for transects measuring one pixel in width). Also included are points corresponding to the bulk porosity and diffusion coefficient calculated for each rock slab (four large symbols).

Figure 1

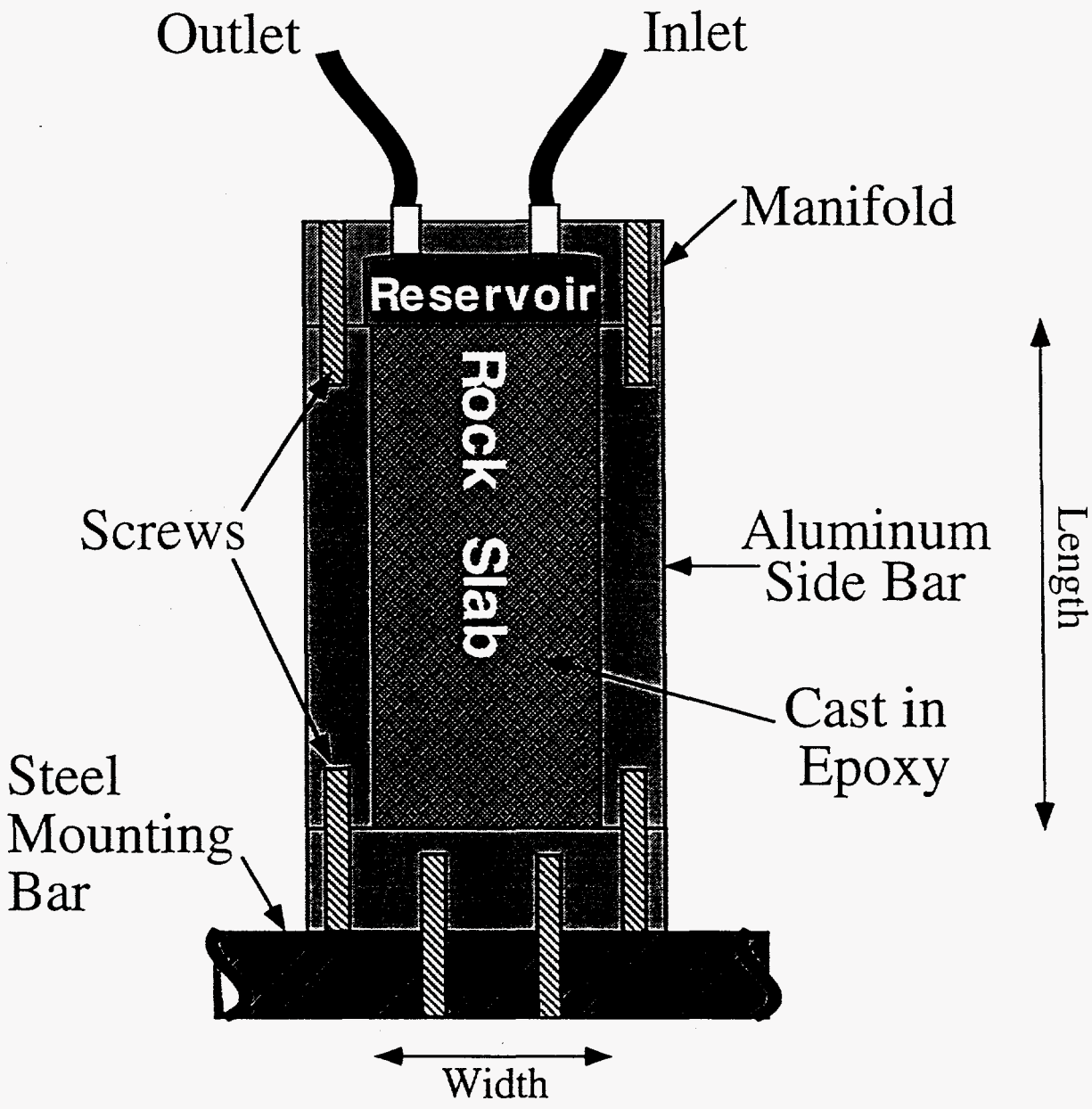

Plan View

Figure 2

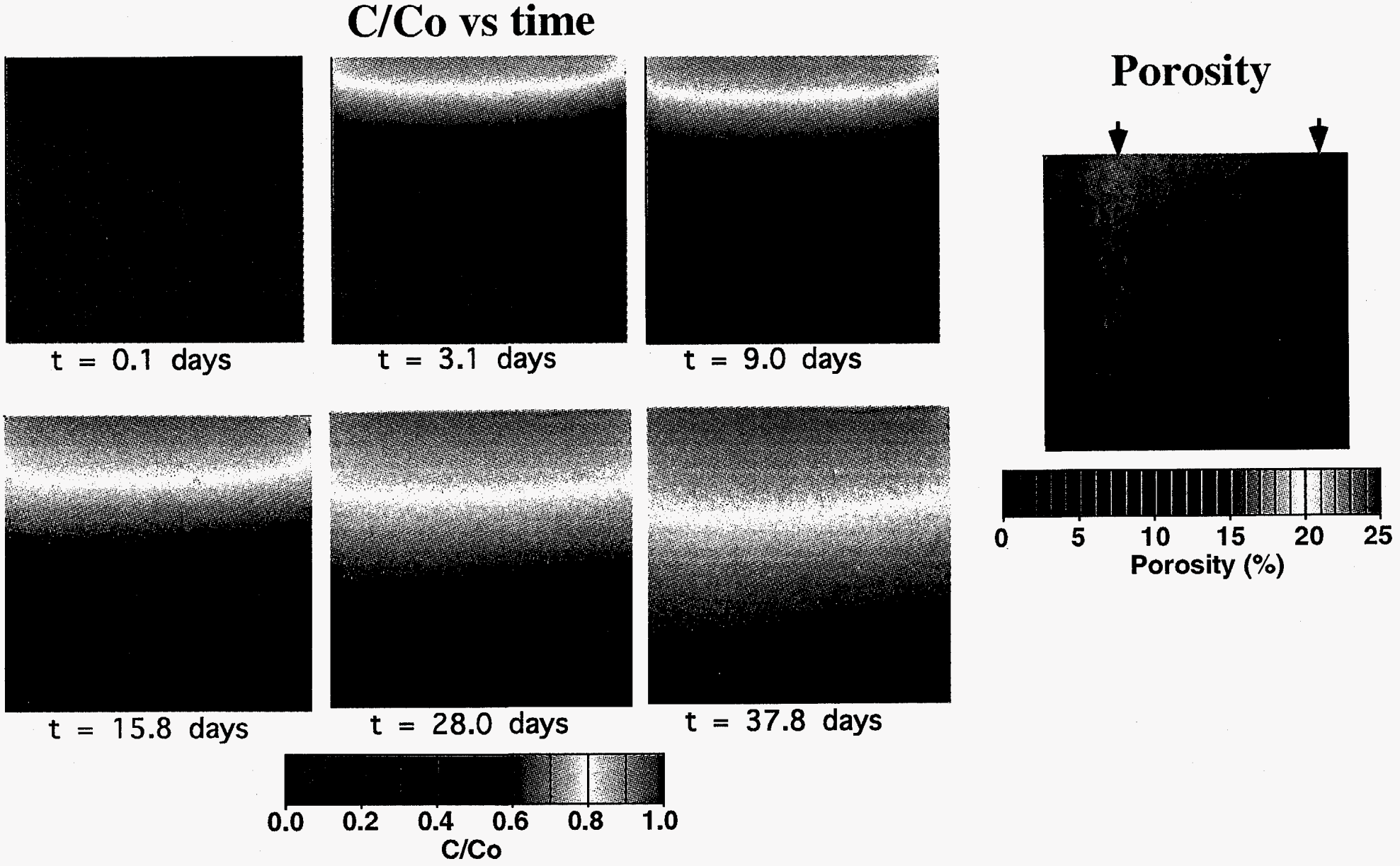
C/Co vs time
t = 0.1 days
t = 3.1 days
t = 9.0 days
t = 15.8 days
t = 28.0 days
t = 37.8 days
0.0
0.2
0.4
0.6
0.8
1.0
C/Co
Porosity
0
5
10
15
20
25
Porosity (%)

Figure 3

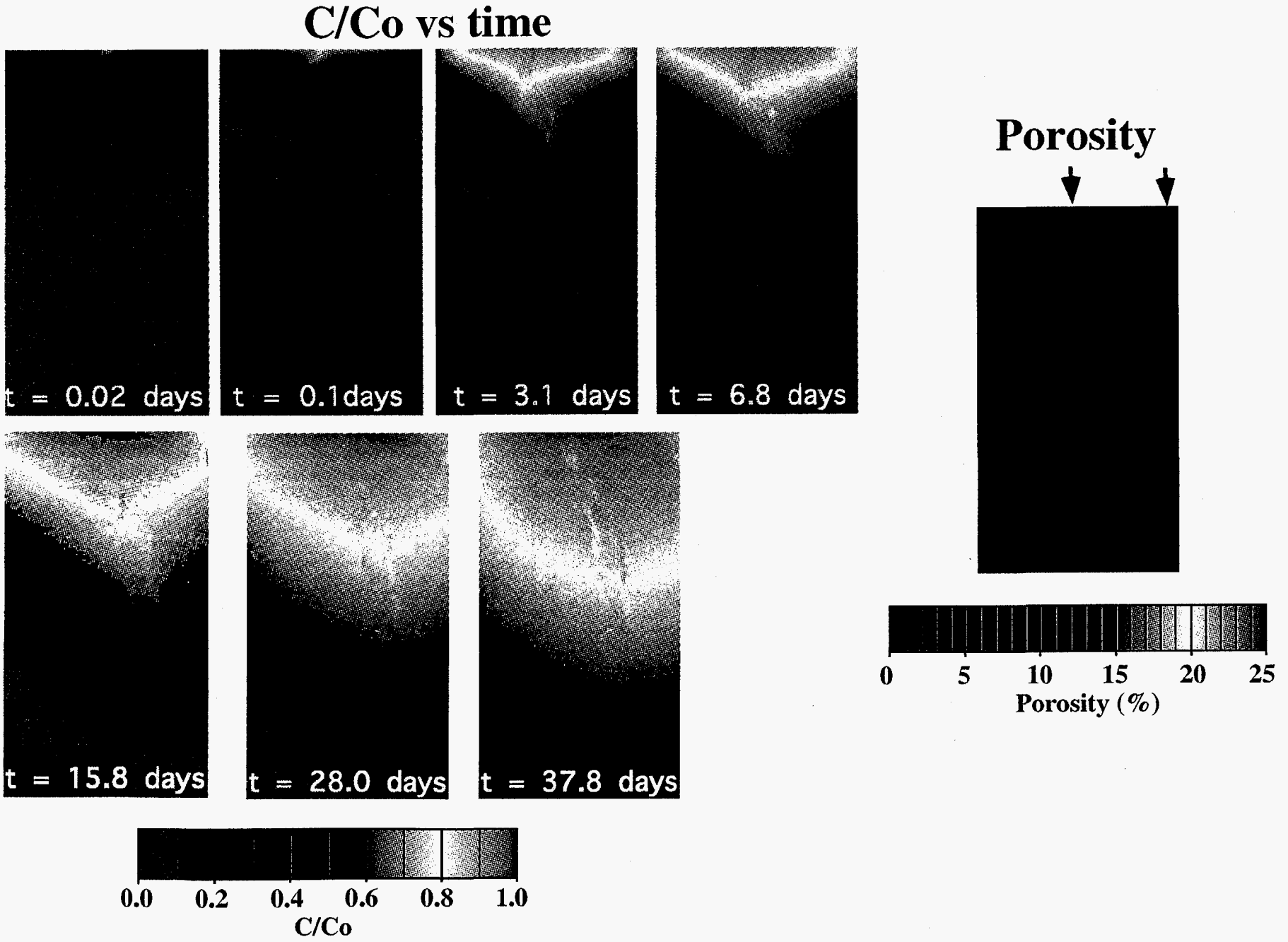
C/Co vs time
t = 0.02 days
t = 0.1days
t = 3.1 days
t = 6.8 days
t = 15.8 days
t = 28.0 days
t = 37.8 days
0.0
0.2
0.4
0.6
0.8
1.0
C/Co
Porosity
0
5
10
15
20
25
Porosity (%)

Figure 4

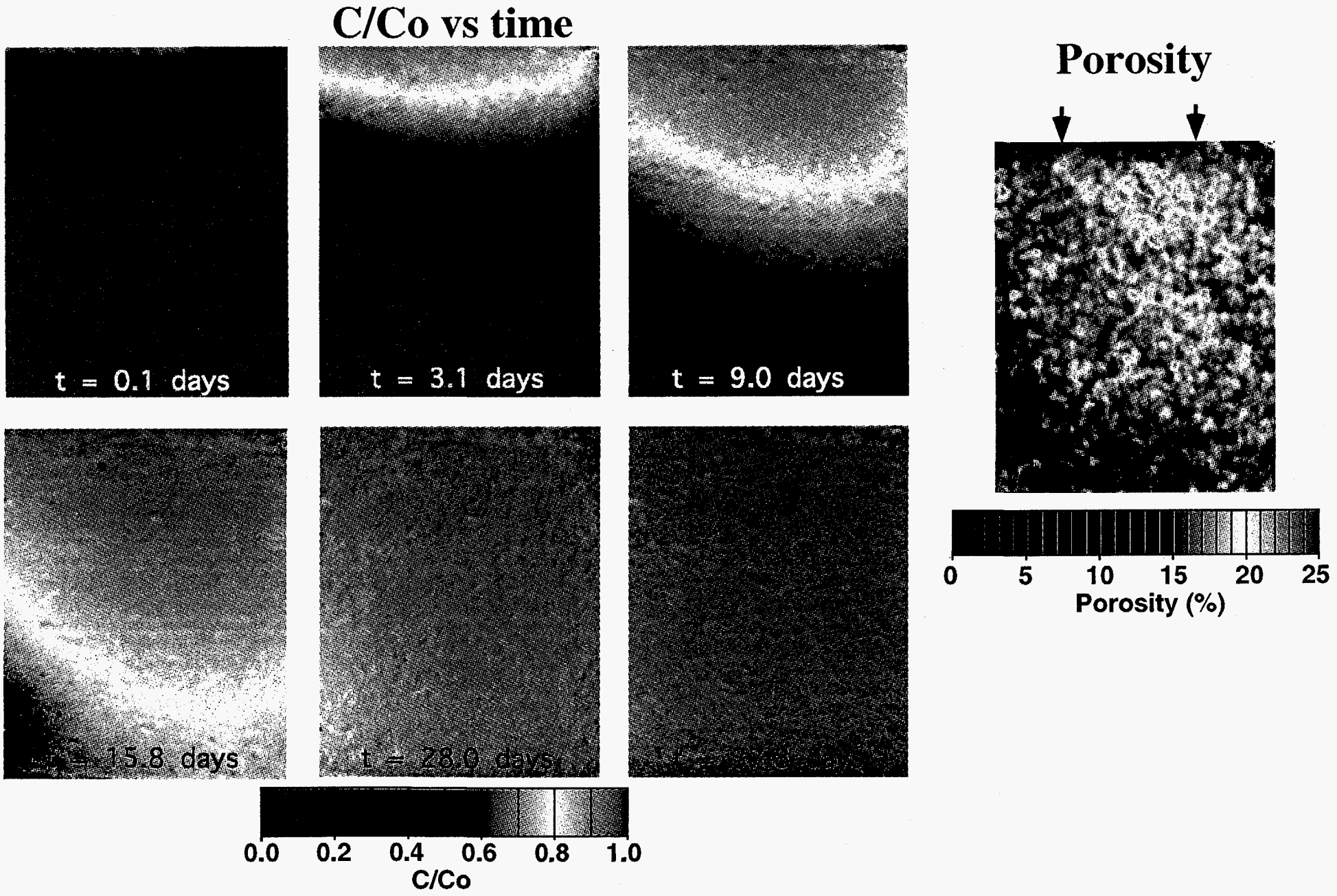
C/Co vs time
t = 0.1 days
t = 3.1 days
t = 9.0 days
t = 15.8 days
t = 28.0 days
0.0
0.2
0.4
0.6
0.8
1.0
C/Co
Porosity
0
5
10
15
20
25
Porosity (%)

Figure 5

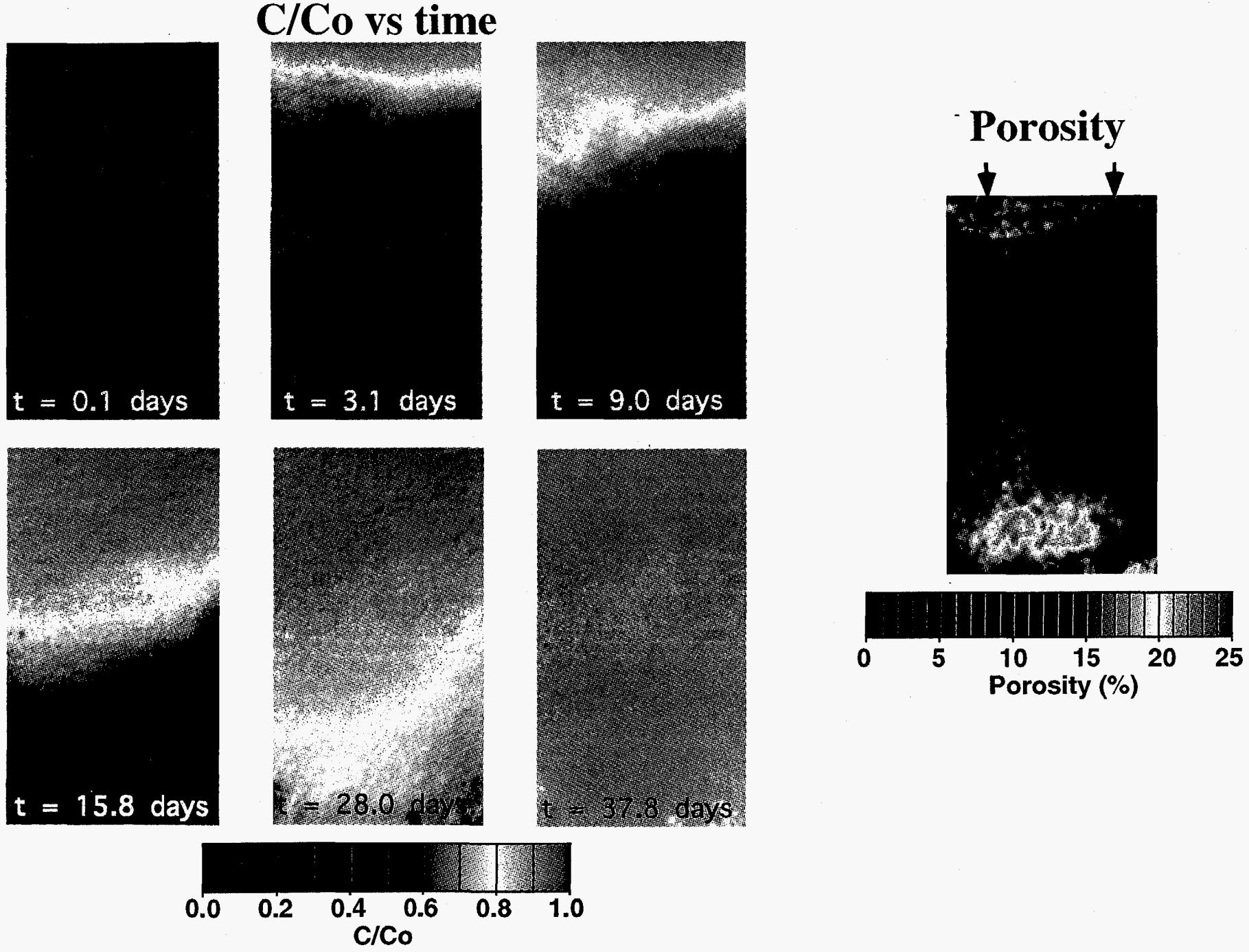
C/Co vs time
t = 0.1 days
t = 3.1 days
t = 9.0 days
t = 15.8 days
t = 28.0 days
t = 37.8 days
0.0
0.2
0.4
0.6
0.8
1.0
C/Co
Porosity
0
5
10
15
20
25
Porosity (%)

Figure 6a

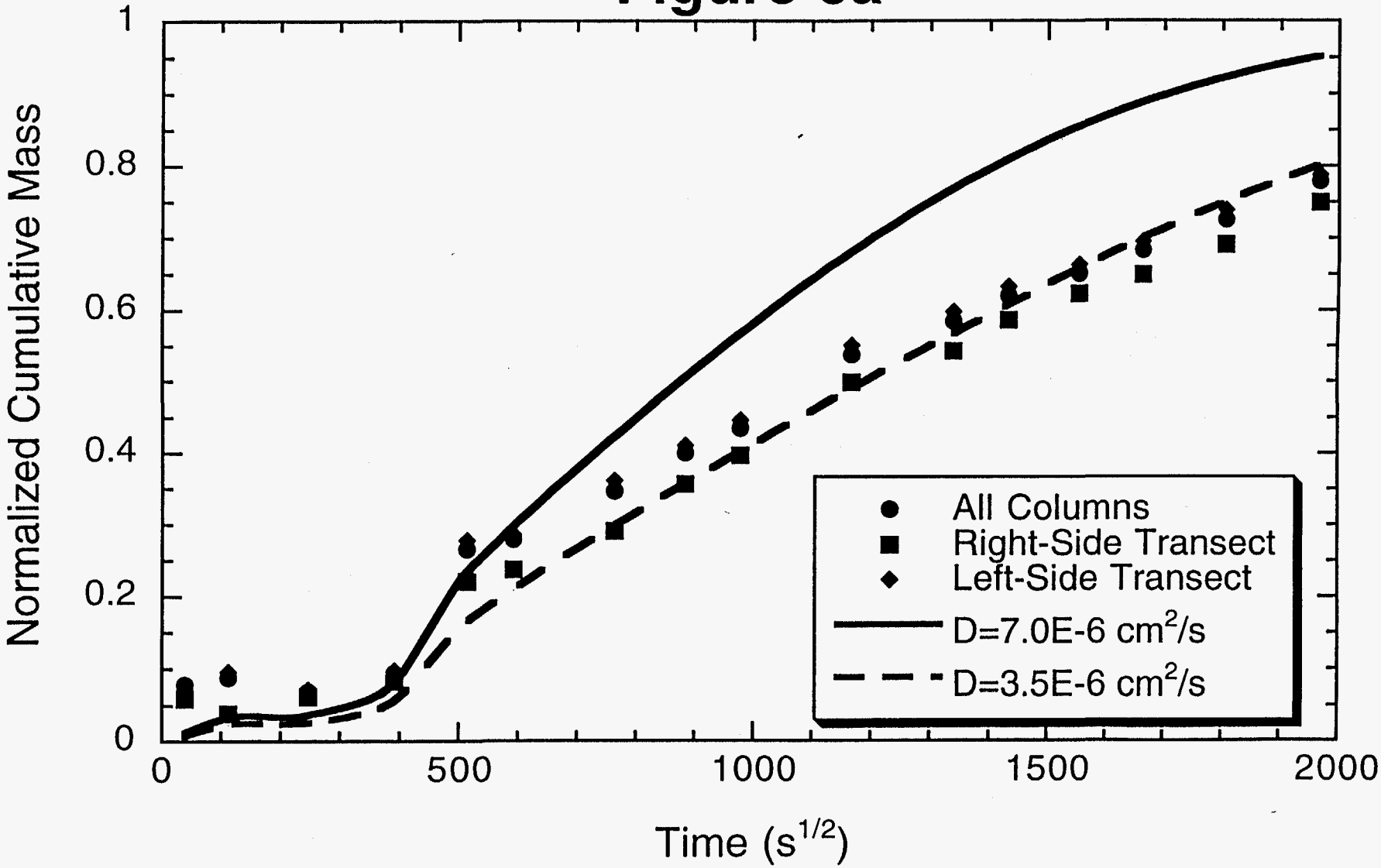
Normalized Cumulative Mass
1
0.8
0.6
0.4
0.2
0
0
500
1000
1500
2000
Time (s^1/2)
All Columns
Right-Side Transect
Left-Side Transect
D=7.0E-6 cm²/s
D=3.5E-6 cm²/s

Figure 6b

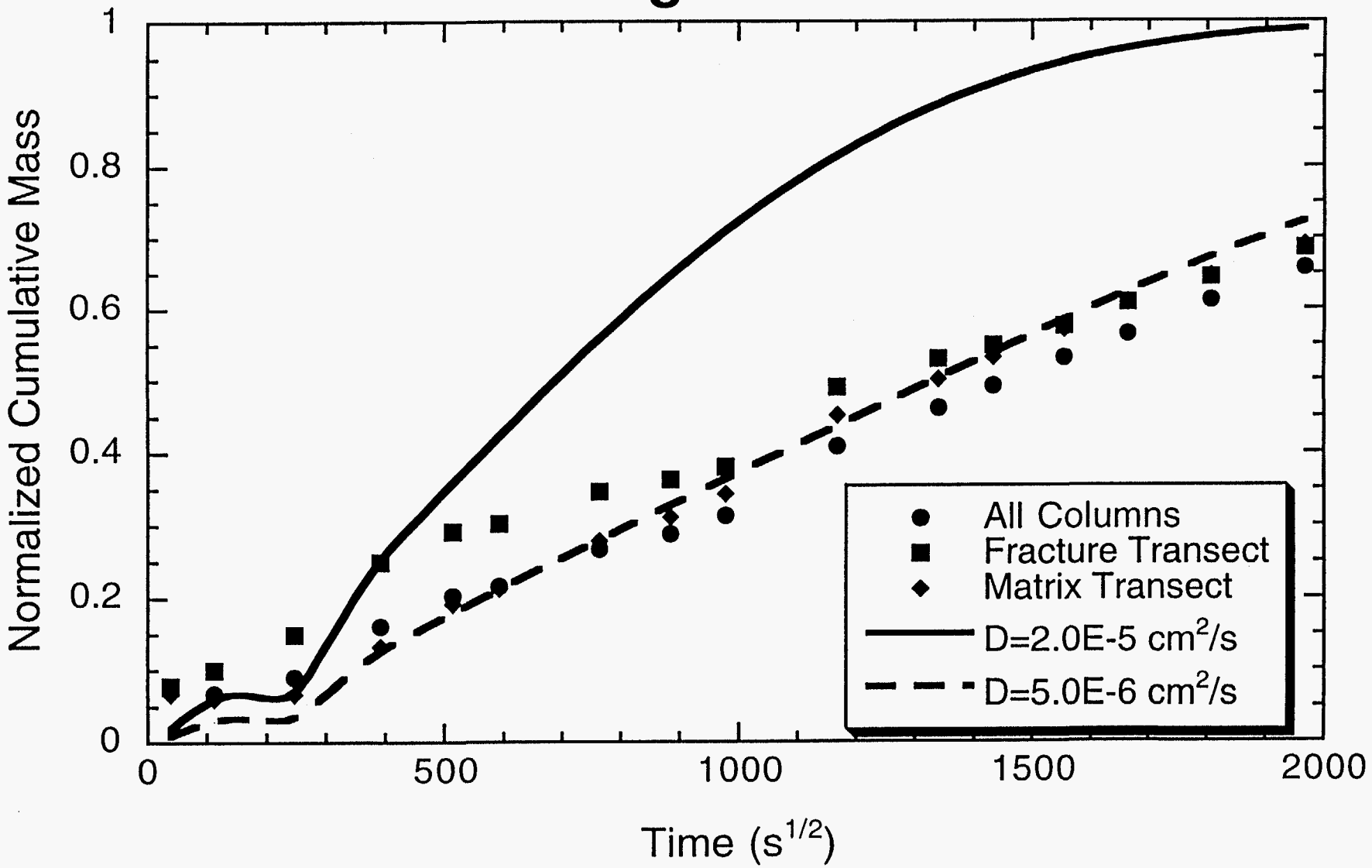
Normalized Cumulative Mass
1
0.8
0.6
0.4
0.2
0
0
500
1000
1500
2000
Time ($s^{1/2}$)
All Columns
Fracture Transect
Matrix Transect
D=2.0E-5 cm^2/s
D=5.0E-6 cm^2/s

Figure 6c

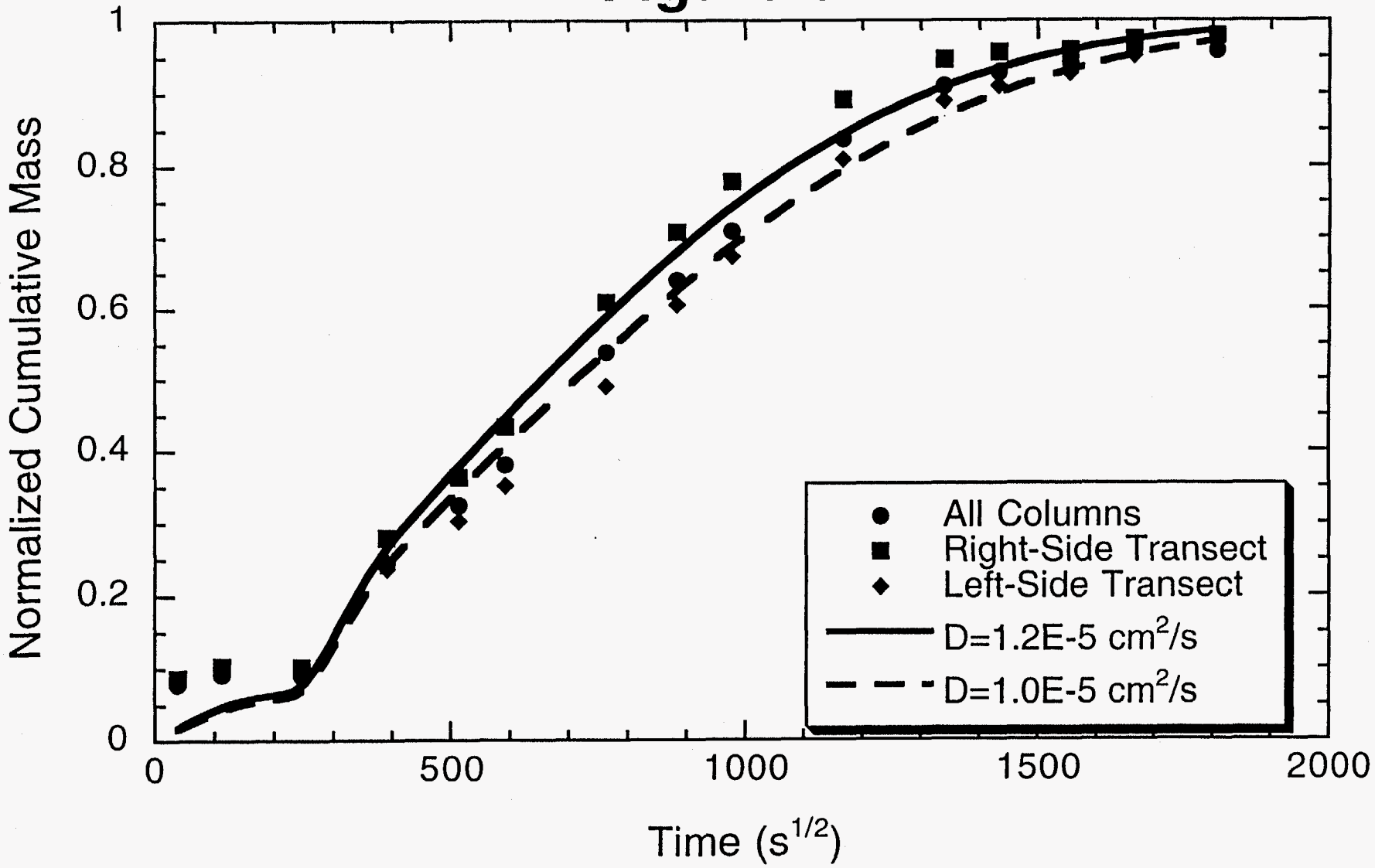
Normalized Cumulative Mass
1
0.8
0.6
0.4
0.2
0
0
500
1000
1500
2000
Time ($s^{1/2}$)
All Columns
Right-Side Transect
Left-Side Transect
D=1.2E-5 cm^2/s
D=1.0E-5 cm^2/s

Figure 6d

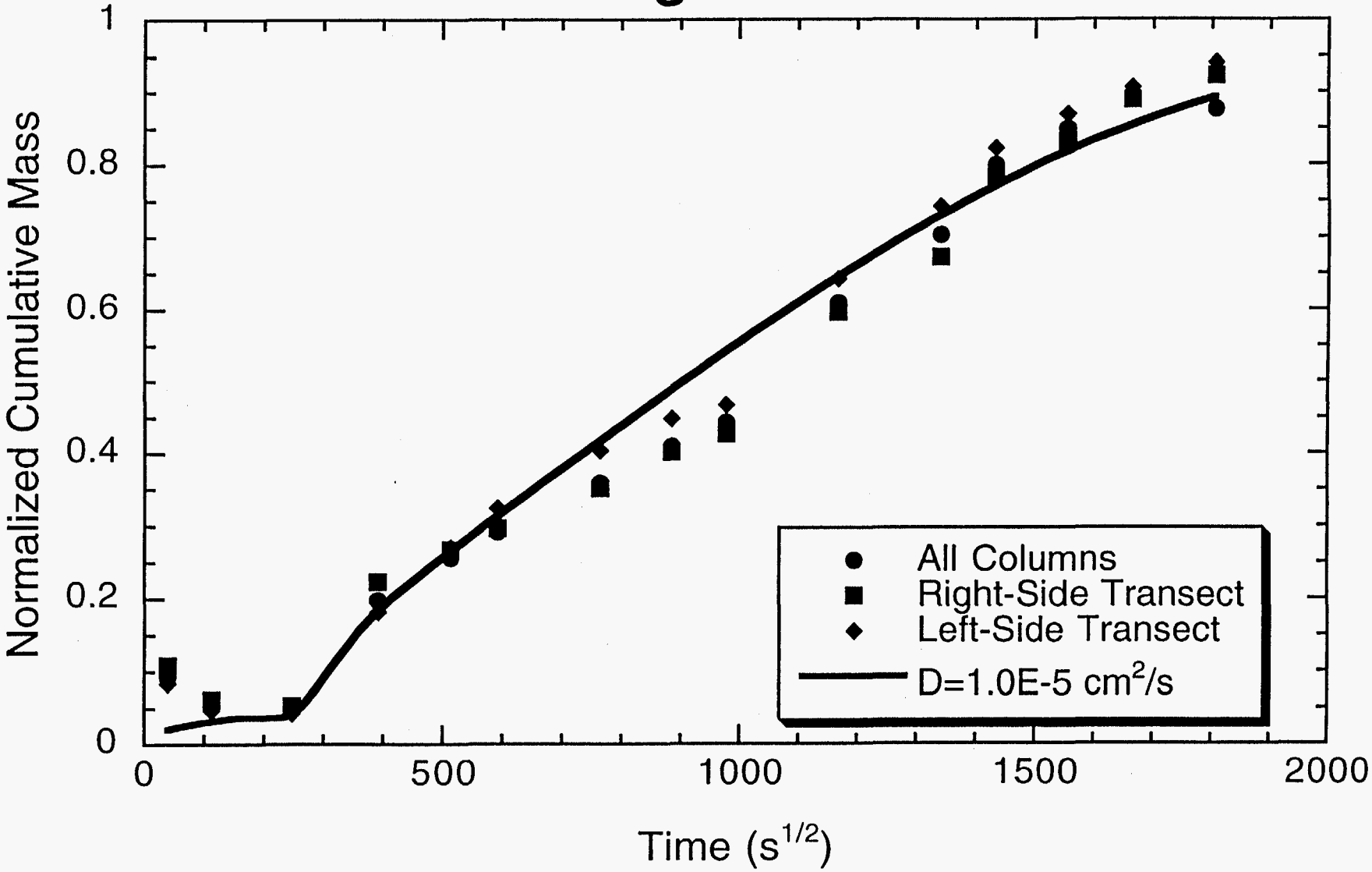
Normalized Cumulative Mass
1
0.8
0.6
0.4
0.2
0
0
500
1000
1500
2000
Time ($s^{1/2}$)
All Columns
Right-Side Transect
Left-Side Transect
D=1.0E-5 cm^2/s

Figure 7

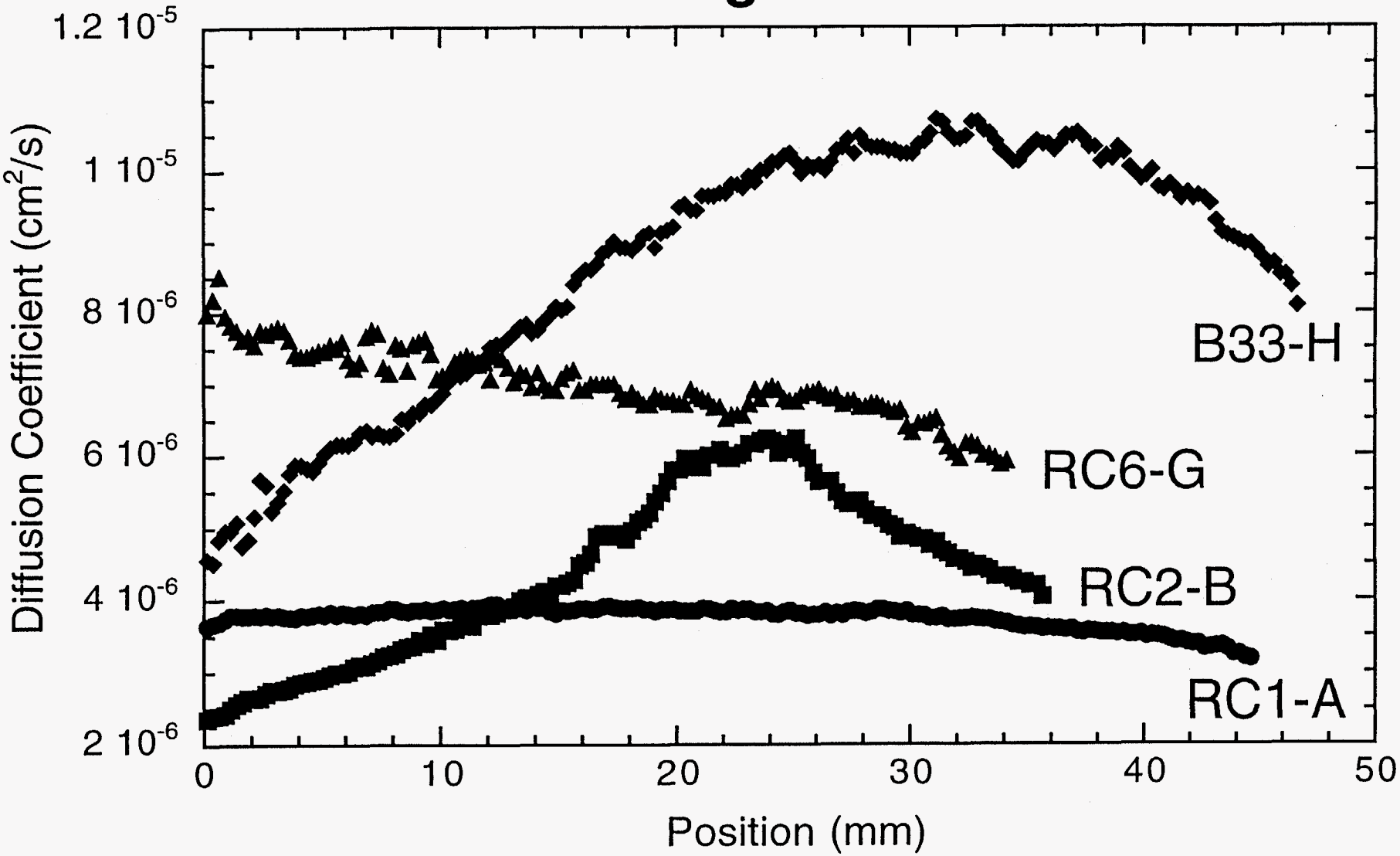
1.2 10-5
1 10-5
8 10-6
6 10-6
4 10-6
2 10-6
Diffusion Coefficient (cm2/s)
0
10
20
30
40
50
Position (mm)
B33-H
RC6-G
RC2-B
RC1-A

Figure 8

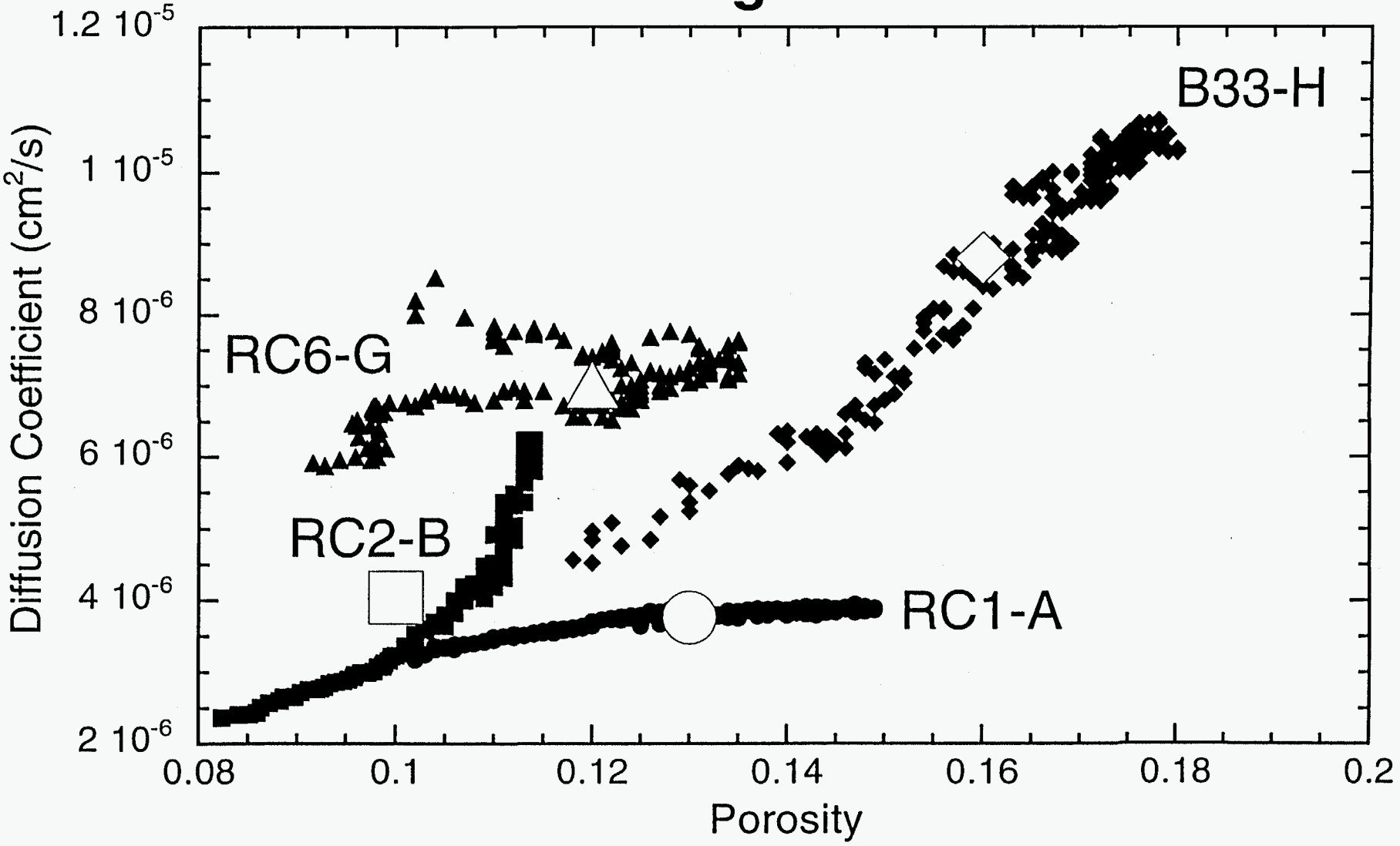
1.2 10-5
1 10-5
8 10-6
6 10-6
4 10-6
2 10-6
Diffusion Coefficient (cm2/s)
0.08
0.1
0.12
0.14
0.16
0.18
0.2
Porosity
B33-H
RC6-G
RC2-B
RC1-A